Line-scan Raman microscopy complements optical coherence tomography for tumor boundary detection

Narendran Sudheendran[1,5], Ji Qi[2,5], Eric D Young[3], Alexander J Lazar[3], Dina C Lev[3], Raphael E Pollock[3], Kirill V Larin[1,4] and Wei-Chuan Shih[1,2]

[1] Department of Biomedical Engineering, University of Houston, 2026 SERC, Houston, TX 77204, USA
[2] Department of Electrical Engineering, University of Houston, N308 Engineering Building 1, Houston, TX 77204, USA
[3] Sarcoma Research Center, The University of Texas MD Anderson Cancer Center, 1515 Holcombe Blvd, Houston, TX 77030, USA
[4] Institute of Optics and Biophotonics, Saratov State University, Saratov 410012, Russia

E-mail: wshih@uh.edu

Abstract

Current technique for tumor resection requires biopsy of the tumor region and histological confirmation before the surgeon can be certain that the entire tumor has been resected. This confirmation process is time consuming both for the surgeon and the patient and also requires sacrifice of healthy tissue, motivating the development of novel technologies which can enable real-time detection of tumor-healthy tissue boundary for faster and more efficient surgeries. In this study, the potential of combining structural information from optical coherence tomography (OCT) and molecular information from line-scan Raman microscopy (LSRM) for such an application is presented. The results show a clear presence of boundary between myxoid liposarcoma and normal fat which is easily identifiable both from structural and molecular information. In cases where structural images are indistinguishable, for example, in normal fat and well differentiated liposarcoma (WDLS) or gastrointestinal sarcoma tumor (GIST) and myxoma, distinct molecular spectra have been obtained. The results suggest LSRM can effectively complement OCT to tumor boundary demarcation with high specificity.

Keywords: tumor-margin, line-scan Raman microscopy, optical coherence tomography

(Some figures may appear in colour only in the online journal)

1. Introduction

Accurate and real-time intraoperative tumor margin assessment is of utmost importance in tissue-preserving surgical procedures such as partial mastectomy for breast cancer [1, 2], prostate [3] and brain tumor excision [4], organ-sparing surgery for liposarcoma [5], and many others. In these surgical procedures, complete excision of the primary tumor is the major determinant of the rate of local cancer recurrence. Minimizing the removal of normal tissue is the main factor in preserving proper organ functions as well as cosmetic appearance. Thus, in successful procedures, complete resection of the cancer must be balanced with tissue conservation. To ensure that all malignant tissue is removed, a small margin of normal tissue surrounding the lesion is excised to ensure that the surgeon removed the entire malignant lesion. Margin status is gauged by pathologic examination of the border of the excised lesion—a two-step process. The first step is intraoperative gross (macroscopic) examination by a surgeon with a naked eye; the second step is postoperative histologic (microscopic) examination using frozen sections stained with hematoxylin and eosin to evaluate a representative area of concern.
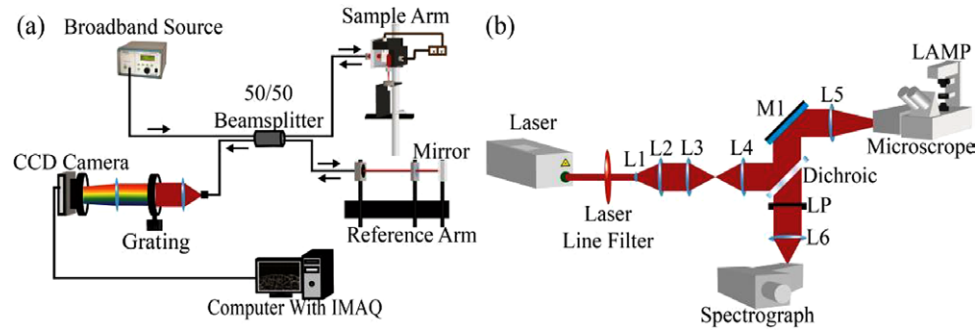
---

[5] These authors contributed equally.

Figure 1. (*a*) Schematic of SDOCT system. (*b*) Schematic of LSRM.

Achieving negative resection margins, typically defined as the absence of malignant tumor cells, provides lower associated rates of future local recurrence [6]. Positive or unknown histological margins usually prompt re-excision surgery because of the elevated risk for local recurrence even when chemo/radiation therapy is administered [7]. In the case of breast cancer, for example, as many as 20%–55% of patients undergoing partial mastectomy require a second surgical procedure due to positive margins indicative of incomplete cancer resection that were missed on intraoperative margin assessment [8].

Currently, a variety of optical imaging and spectroscopic techniques are being explored to improve cancer diagnosis. However, the application of these methods for intraoperative surgical margin assessment is very limited. Preliminary *in vivo* results have shown the efficacy of diffuse reflectance spectroscopy in the diagnosis of breast lesions, as well as in the assessment of tumor margins [9]. This technique has shown great promise in the assessment of large-volume tumors, but cannot provide localized information regarding tumor margins due to low resolution. Optical coherence tomography (OCT), in contrast, can provide high resolution images in 3D [10]. Other than structural imaging, OCT has also been demonstrated for flow measurements using Doppler information [11, 12]. Phase-sensitive OCT has been used for assessing biomechanical properties of tissues previously [13]. OCT has also been applied in the field of embryology [14, 15]. OCT has also been used for monitoring changes in optical properties due to applications of chemicals such as glucose and glycerol [16, 17], and this has further been extended to differentiate cancerous tissues from normal ones [18, 19]. Raman spectroscopy, on the other hand, has been employed to identify intraoperative margin based on tissue variations at the molecular level [8]. A dual-mode system has been developed to collect point-wise Raman spectra and OCT images from biological tissue [20–22]. Another application that combines OCT and Raman spectroscopy has been recently developed by us [23].

In this study, we present the first application of combining information from line-scan Raman microscopy (LSRM) and optical coherence tomography (OCT) imaging for the assessment of diseased/normal boundary. Raman imaging has been a time-consuming process. Recent progress has been made to take advantage of parallel acquisition in the form of line-scan (LSRM) and active-illumination [24]. As described in a recent paper, LSRM enables the parallel acquisition of microscopic

Raman spectra from ~133 spots of $1\,\mu m^2$ each. In other words, LSRM provides concurrent Raman mapping along a straight line without the need for scanning. To obtain Raman maps over a 2D region of interest, only scanning along the transverse direction of the projected laser line is needed. Therefore, an effective data acquisition speed ~133 times faster than a point-scan confocal Raman microscope can be obtained [25]. LSRM has been shown to provide rapid acquisition of images of population-level living cells without pre-photobleaching. Since Raman spectroscopy is sensitive to tissue molecular composition, while OCT can detect structural changes, these two modalities provide complementary information. In addition, since both LSRM and OCT utilize tissue intrinsic contrasts, no staining, fixation or exogenous markers are needed, a critical advantage for potential clinical application. Further, unlike in previous attempts, the Raman modality is implemented here as an imaging tool with parallel data acquisition. The high-throughput properties of this technology allow us to obtain, for the first time, an image across the disease/normal boundary without scanning.

2. Materials and methods

2.1 SDOCT system

A spectral domain OCT (SDOCT) system was used for this study (figure 1(*a*)). The system comprises of a broadband superluminescent laser diode (broadlighter S840, Superlum, Russia, 840 ± 25 nm wavelength range, 20 mW output power) at the source end, Michelson interferometer with 50/50 split ratio to the sample and reference arms and a spectrometer at the detector end. The spectrometer comprises of a diffraction grating (Wasatch Photonics, 1200 grooves mm^{-1}) and a CCD line scan camera (Basler L104K, 2048 pixel resolution, 29.3 kHz line rate). The interference signal from the sample and the reference arms of the Michelson interferometer is detected by the spectrometer and digitized by an image acquisition card (NI-IMAQ PCI-1428). Depth profile (A-line) is obtained by converting the interference signal detected by the IMAQ into linear *k*-space and then performing fast Fourier transform (FFT) algorithm on it. 3D imaging is performed by scanning the laser beam across the surface of the sample, at the sample arm, using galvanometer mounted mirrors. The SDOCT system has an axial (at 3 dB drop) and transverse resolution of 8 μm and an imaging depth of 4.5 mm (in air).

2.2 Line-scan Raman microscopy (LSRM) system

The LSRM system used in this study is described in figure 1(*b*) [25]. We employ a CW Titanium:Sapphire laser (Spectra-Physics 3900 S) pumped by a diode-pumped solid state green laser (Spectra-Physics Millennia X). The 785 nm output is filtered by a 785 nm laser line filter (Semrock LL01-785-12.5). The laser output is transformed by a line-generating optical system consisting of a Powell lens and two cylindrical lenses to form a uniform line, which is 133 μm long. This line is relayed to the side-port focal plane of an inverted microscope (Olympus IX71). A dichroic beamsplitter (Semrock LPD01-785RU-25) is placed on the beam path to reflect the laser light. Epi-Raman is collected by a microscope objective (Olympus UPLSAPO 60XW) and sent through the dichroic beamsplitter and a long-wave pass filter (Semrock LP02-785RS-25) for laser intensity reduction, and imaged at the entrance slit of a spectrograph with a CCD detector (Princeton LS785). Full-frame data of dimension 133 (spatial) $\times$ 1340 (λ) are collected, equivalent to 133 'point-spectra', each from a 1 μm^2 spot. The spatial resolution of the system is 0.6 μm $\times$ 0.8 μm. The spectral resolution is 8 cm^{-1}.

2.3 Sample preparation

Tissue samples were obtained after surgical resection at The University of Texas, M.D Anderson Cancer center (UTMDACC) hospital under an IRB approved protocol with patient consent, stored in sterile phosphate buffered saline (PBS) and imaged using SDOCT system on the same day. A small part of the sample was dissected to be imaged by the RSI. The rest of sample was fixed in formalin and prepared for histological analysis. Tissue samples to be imaged by line scan Raman system were placed onto No.1 coverslips and fixed at the sample holder of microscope. The total acquisition time for each spectrum is 60 s at a power density of 1 mW μm^{-2}. The Protocols for tissue processing were approved by the University of Houston Biosafety committee.

3. Results and discussion

In this study, we present the prospect of combining structural information from OCT and molecular information from LSRM, for tumor border identification during tumor resection surgeries. The similarity between OCT structural images and H&E histology images of normal fat, well differentiated liposarcoma (WDLS) and dedifferentiated liposarcoma (DDLS) has already been shown previously [26]. These results suggested that the structural differences between normal fat, WDLS and DDLS are easily identifiable from their corresponding OCT structural images. Hence, OCT can be used for used for gross inspection of tumor margins. However, in cases where differences in OCT structural images are not very obvious, LSRM can be used for confirming the molecular information from the suspicious regions. To check consistency, Raman spectra were obtained from 7 different samples of normal fat tissue. The averaged Raman spectral information from normal fat samples is depicted in figure 2. The gray shade represents the ±1 standard deviation that is less than ±5%.

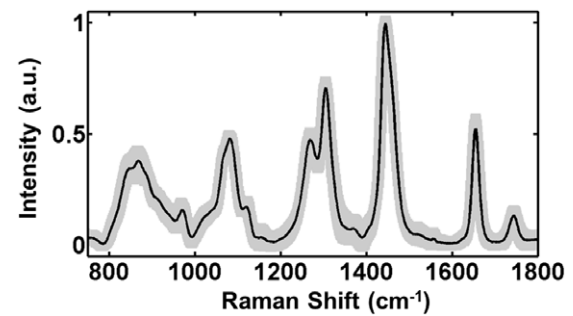**Figure 2.** Average Raman spectra from normal fat tissue with the gray shade representing ±1 standard deviation.

Figures 3(*a*) and (*b*) show OCT structural image and the corresponding H&E histology of myxoid liposarcoma respectively. Myxoid liposarcoma is comprised of copious amorphous mucoid material with admixed small, stubby spindle cells and a variable number of neoplastic adipocytes of various sizes [27], as evident by the white and black arrows in figures 3(*a*) and (*b*), respectively. Figure 3(*c*) is a representative OCT structural image of normal surrounding fat tissue. The margin between normal fat and myxoid liposarcoma is shown by the white arrow in figure 3(*d*). There is a clear difference in the OCT structural images between normal fat and myxoid liposarcoma. This obvious difference in structures will be very helpful to the surgeon to determine the tumor margin while performing resection surgery. We also studied capability of LSRM to differentiate between normal tissue and tumor regions. A bright field microscopic image of the surface of the sample was captured by a CMOS camera which is shown in figure 4(*a*). The black dashed curve on figure 4(*a*) indicates the boundary between myxoid liposarcoma (Region 1) and normal fat (Region 2). The laser line projection on the sample, imaged by the LSRM, is indicated by the solid red line in figure 4(*a*). We emphasize that spatially resolved Raman spectra from this entire line (133 μm long) were captured in one CCD image of Raman shift (*x*-axis) and spatial coordinates (*y*-axis) (figure 4(*b*)). The spectra from the abnormal region have lower Raman intensity compared to the normal spectra, possibly due to the lack of cellular structures and thus less elastic back scattering, agreeing with the OCT measurements. Figure 4(*c*) compares the spectra, averaged over 21 spectra from cancerous region (A) and the normal region (B) respectively, These spectra are post-processed by first subtracting a glass coverslip fluorescence background followed by an automated background subtraction method [28]. Comparing the normal and the abnormal spectra, the intensity ratio of lipid bands at 1448 cm^{-1} (CH$_2$ bending) and 1655 cm^{-1} (C=C stretching) changes from 2:1 in the normal to 1:1 in the abnormal region, agreeing with previous studies [29]. Biochemically, this agrees with the decrease in the ratio of monounsaturated lipids to polyunsaturated fatty acyl chains of lipids in liposarcoma compared to normal tissue [30, 31]. We also observe the broadening of the 1655 cm^{-1} peak in the abnormal region. A Raman spectrum acquired from a separate healthy tissue is shown in figure 4(*d*), which appears to be virtually identical to trace B in figure 4(*c*).
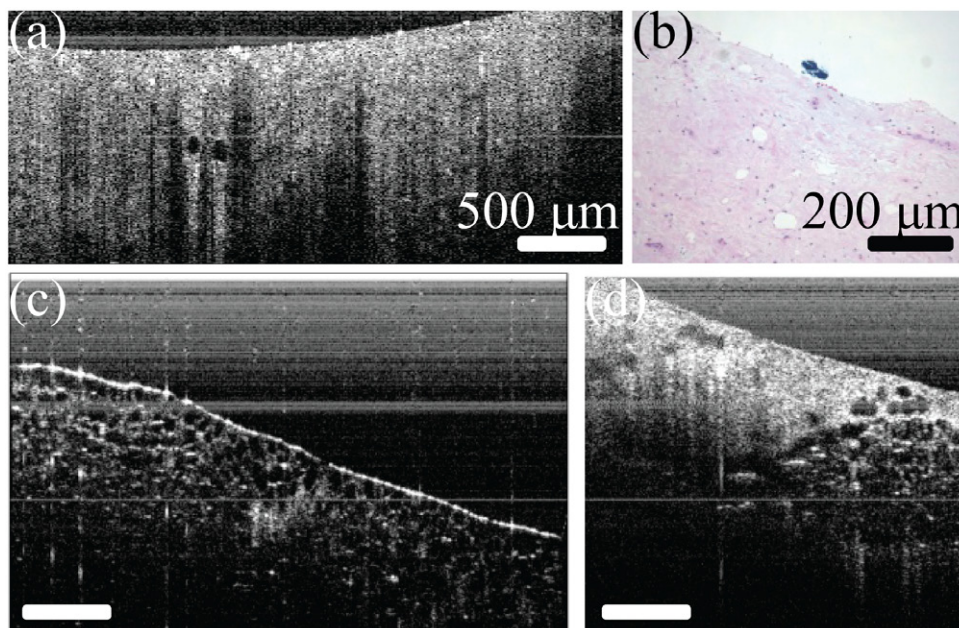
Figure 3. (*a*) 2D OCT structural image of myxoid liposarcoma. (*b*) H&E histology section corresponding to (*a*). (*c*) 2D OCT structural image of normal fat. (*d*) 2D OCT structural image depicting boundary between myxoid liposarcoma and normal fat.
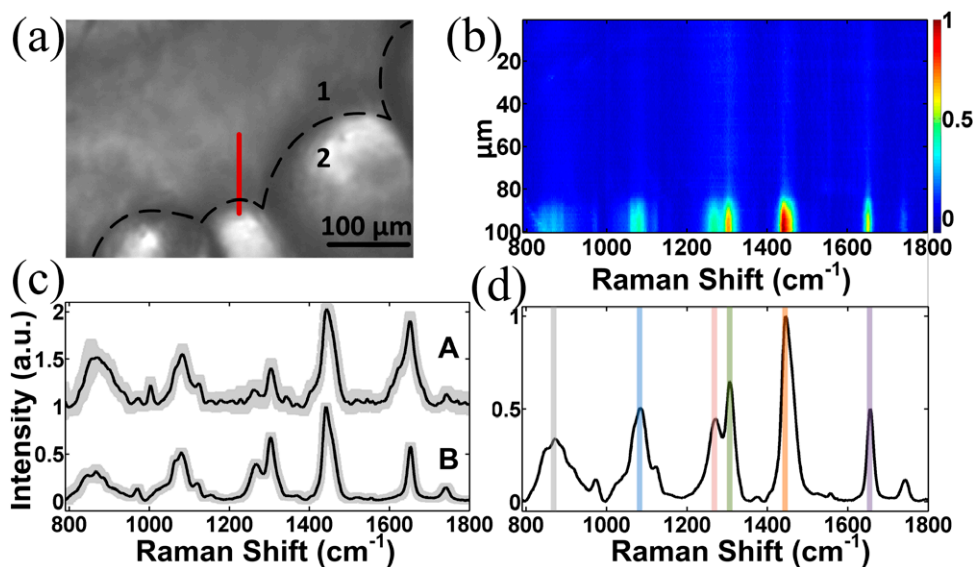

Figure 4. (*a*) Photograph of the tissue imaged by LSRM. Black dashed line indicates boundary between myxoid liposarcoma (Region 1) and normal fat (Region 2). (*b*) LSRM image corresponding to red line in (*a*). (*c*) Averaged Raman spectrum from regions corresponding to myxoid liposarcoma (A) and normal fat (B). (*d*) Averaged Raman spectrum from a different homogenous normal fat tissue.

In the case of myxoid liposarcoma and normal fat tissue, the differences in their corresponding OCT structural images (figure 3) are obvious by visual inspection and their corresponding LSRM image (figure 4) further supports the diagnosis. However, the difference between normal fat and WDLS cannot be confirmed by visual inspection of their corresponding OCT structural images (figures 5(*a*) and (*b*)). However, LSRM can provide critical intrinsic chemical composition information that would identify WLDS and normal fat. Figure 5(*c*) presents the Raman spectra from WLDS (black) and normal fat sample (red). The Raman

spectra shown here are averaged from 80 different locations and normalized to Raman bands at $1448 \, \text{cm}^{-1}$ (CH_2 bending). Broadening of $1655 \, \text{cm}^{-1}$ and decrease of $1655 \, \text{cm}^{-1}$ (C=C stretching) and $1734 \, \text{cm}^{-1}$ (C=O stretching [32]) in WDLS are observed. Although tissue Raman spectra are highly complex and typically requires advanced chemometrics [33, 34], we have obtained highly-distinguishable spectra from fat and WDLS. Thus, univariate statistical analyses are effective to quantify the difference between WDLS and normal fat tissue. The histogram of peak area under $1655 \, \text{cm}^{-1}$ is shown in figure 5(*d*), where a threshold of 15.5
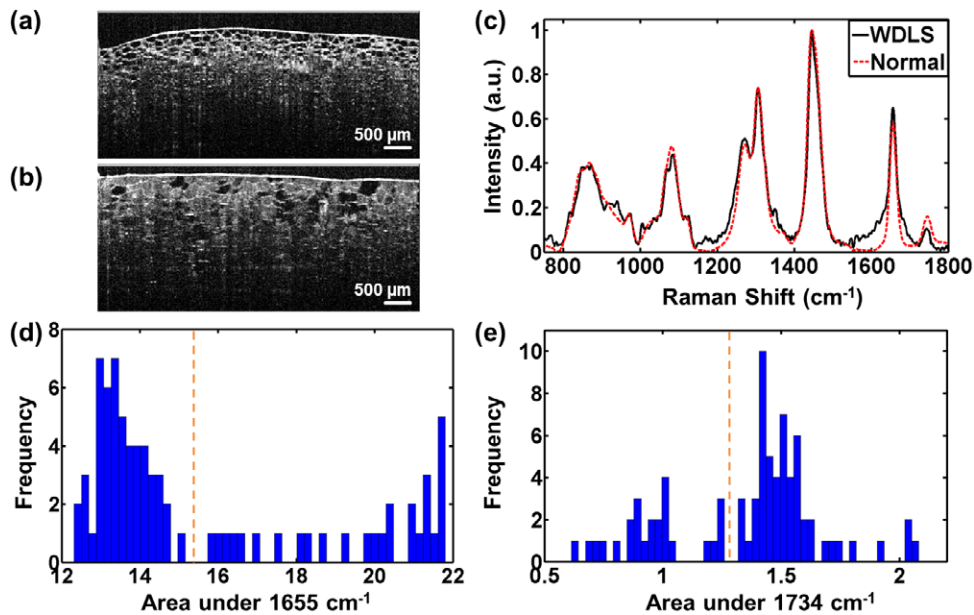
Figure 5. OCT images from normal fat tissue (*a*) and WDLS (*b*); (*c*) Raman spectra from normal fat tissue (red dotted) and WDLS (black); the spectra are normalized to $1440 \, cm^{-1}$; histogram of area under Raman bands at $1655 \, cm^{-1}$ (*d*) and $1734 \, cm^{-1}$ (*e*), the spectra are normalized to $1655 \, cm^{-1}$ band. The orange dotted lines present the threshold to separate normal fat tissue and WDLS.
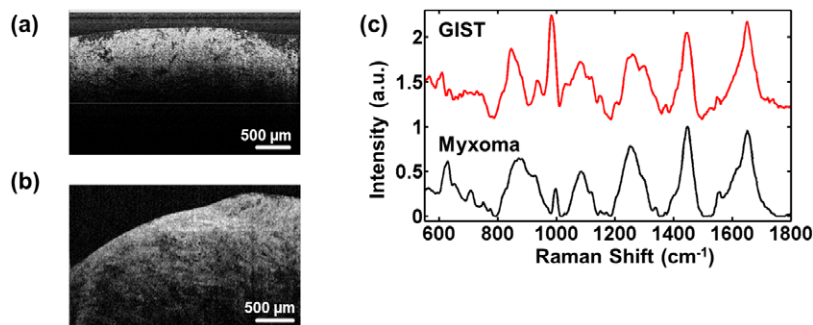

Figure 6. OCT images from gastrointestinal sarcoma tumor (*a*) and myxoma (*b*); (*c*) Raman spectra from myxoma (red) and GIST (black).

can seperate WDLS from normal fat tissue, as indicated by a dashed orange line. Spectra with peak area larger than 15.5 are identified as WDLS with a *p*-value less than 0.01. We also use peak area under $1734 \, cm^{-1}$ to differentiate WDLS and normal fat, as shown in figure 5(*e*), where a threshold of 1.28 can be used to separate WDLS and normal fat. Spectra with peak area of less than 1.28 are identified as WDLS with an associated *p*-value less than 0.01.

Similarly, there is no clear distinction between gastrointestinal sarcoma tumor (GIST) and myxoma from their corresponding OCT structural images (figures 6(*a*) and (*b*)). However, Raman spectra acquired from GIST (red) and myxoma (black) show different chemical features as shown in figure 6(*c*). Both spectra are normalized to Raman bands at $1448 \, cm^{-1}$ (CH_2 bending). GIST shows a stronger band around $1000 \, cm^{-1}$ (CC aromatic ring breathing [35]). Raman bands at $845 \, cm^{-1}$ (CCH aromatic deformation), $935 \, cm^{-1}$ (CCH deformation), $1028 \, cm^{-1}$ (CH stretching), $1261 \, cm^{-1}$ (Amide III) and $1302 \, cm^{-1}$ (Palmitic acid) are not observed in myxoma [35]. Spectrum acquired from myxoma also shows distinct features at $750 \, cm^{-1}$ (symmetric ring breathing), $774 \, cm^{-1}$ (ring vibration), $1254 \, cm^{-1}$ (CH_2 in plane) and $1340 \, cm^{-1}$ (CH_2 deformation [35]). Both spectra show a 1:1 intensity ration of lipid bands at $1448 \, cm^{-1}$ and $1655 \, cm^{-1}$ and a broadening at $1655 \, cm^{-1}$. These distinct Raman features can effectively differentiate GIST from myxoma.

4. Conclusions

In cases where OCT images are indistinguishable, for example, in normal fat and well differentiated liposarcoma (WDLS) or gastrointestinal sarcoma tumor (GIST) and myxoma, distinct Raman spectra have been obtained. The results suggest LSRM can effectively complement OCT to tumor boundary demarcation with high specificity. In this study, the tissue samples were imaged on separate SDOCT and LSRM systems, but our future studies will focus on combining OCT and LSRM system into a single probe based system that can be used for real-time application during tumor resection surgeries.

References

[1] Anscher M S *et al* 1993 *Ann. Surg.* **218** 22–8

[2] Roukos D H, Kappas A M and Agnantis N J 2003 *Ann. Surg. Oncol.* **10** 718–21

[3] Lawrentschuk N, Evans A, Srigley J, Chin J L, Bora B, Hunter A, McLeod R and Fleshner N E 2011 *Cuaj-Can. Urol. Assoc. J.* **5** 161–6

[4] Lin W C, Toms S A, Johnson M, Jansen E D and Mahadevan-Jansen A 2001 *Photochem. Photobiol.* **73** 396–402

[5] Katz M H, Choi E A and Pollock R E 2007 *Expert Rev. Anticancer Ther.* **7** 159–68

[6] Park C C *et al* 2000 *J. Clin. Oncol.* **18** 1668–75

[7] Walls J, Knox F, Baildam A D, Asbury D L, Mansel R E and Bundred N J 1995 *Ann. R. Coll. Surg. Engl.* **77** 248–51

[8] Haka A S, Shafer-Peltier K E, Fitzmaurice M, Crowe J, Dasari R R and Feld M S 2005 *Proc. Natl. Acad. Sci. USA* **102** 12371–6

[9] Bigio I J, Bown S G, Briggs G, Kelley C, Lakhani S, Pickard D, Ripley P M, Rose I G and Saunders C 2000 *J. Biomed. Opt.* **5** 221–8

[10] Huang D, Swanson E, Lin C, Schuman J, Stinson W, Chang W, Hee M, Flotte T, Gregory K and Puliafito C 1991 *Science* **254** 1178–81

[11] Bonesi M, Churmakov D Y, Ritchie L J and Meglinski I V 2007 *Laser Phys. Lett.* **4** 304–7

[12] Veksler B, Kobzev E, Bonesi M and Meglinski I 2008 *Laser Phys. Lett.* **5** 236–9

[13] Jiasong L, Shang W, Singh M, Aglyamov S, Emelianov S, Twa M D and Larin K V 2014 *Laser Phys. Lett.* **11** 065601

[14] Larina I V, Carbajal E F, Tuchin V V, Dickinson M E and Larin K V 2008 *Laser Phys. Lett.* **5** 476–9

[15] Sudheendran N, Syed S H, Dickinson M E, Larina I V and Larin K V 2011 *Laser Phys. Lett.* **8** 247–52

[16] Ghosn M G, Syed S H, Befrui N A, Leba M, Vijayananda A, Sudheendran N and Larin K V 2009 *Laser Phys.* **19** 1272–5

[17] Larin K V, Ghosn M G, Ivers S N, Tellez A and Granada J F 2007 *Laser Phys. Lett.* **4** 312–7

[18] Zhong H Q, Guo Z Y, Wei H J, Si J L, Guo L, Zhao Q L, Zeng C C, Xiong H L, He Y H and Liu S H 2010 *Laser Phys. Lett.* **7** 388–95

[19] Zhong H Q, Guo Z Y, Wei H J, Zeng C C, Xiong H L, He Y H and Liu S H 2010 *Laser Phys. Lett.* **7** 315–20

[20] Patil C A, Bosschaart N, Keller M D, van Leeuwen T G and Mahadevan-Jansen A 2008 *Opt. Lett.* **33** 1135–7

[21] Patil C A, Kalkman J, Faber D J, Nyman J S, van Leeuwen T G and Mahadevan-Jansen A 2011 *J. Biomed. Opt.* **16** 011007

[22] Patil C A, Kirshnamoorthi H, Ellis D L, van Leeuwen T G and Mahadevan-Jansen A 2011 *Lasers Surg. Med.* **43** 143–51

[23] Liu C-H, Qi J, Lu J, Wang S, Wu C, Shih W-C and Larin K V 2014 *J. Innovative Opt. Health Sci.* 140601175004007

[24] Qi J and Shih W C 2012 *Opt. Lett.* **37** 1289–91

[25] Qi J and Shih W-C 2014 *Appl. Opt.* **53** 2881–5

[26] Carbajal E F, Baranov S A, Manne V G R, Young E D, Lazar A J, Lev D C, Pollock R E and Larin K V 2011 *J. Biomed. Opt.* **16** 020502

[27] Loubignac F, Bourtoul C and Chapel F 2009 *World J. Surg. Oncol.* **7** 42

[28] Qi J, Li J T and Shih W C 2013 *Biomed. Opt. Express* **4** 2376–82

[29] Manoharan R, Wang Y and Feld M S 1996 *Spectrochim. Acta* A **52** 215–49

[30] Halliday K R, Sillerud L O and Fenoglio-Preiser C 1989 *Adv. Pathol.* **2** 213–58

[31] Mizuno A, Hayashi T, Tashibu K, Maraishi S, Kawauchi K and Ozaki Y 1992 *Neurosci. Lett.* **141** 47–52

[32] Thakur J S *et al* 2007 *J. Raman Spectrosc.* **38** 127–34

[33] Shih W C, Bechtel K L and Feld M S 2007 *Anal. Chem.* **79** 234–9

[34] Shih W C, Bechtel K L and Feld M S 2008 *Opt. Express* **16** 12726–36

[35] Huang N Y, Short M, Zhao J H, Wang H Q, Lui H, Korbelik M and Zeng H S 2011 *Opt. Express* **19** 22892–909